Rotational Structure and Dissociation of the Rydberg States of CO Investigated by Ion-dip Spectroscopy

doi: 10.1063/1.469665

Rotational structure and dissociation of the Rydberg states of CO investigated by ion-dip spectroscopy

Masaaki Komatsu, Takayuki Ebata, Toshihiko Maeyama, and Naohiko Mikami
Department of Chemistry, Faculty of Science, Tohoku University, Sendai 980-77, Japan

(Received 28 February 1995; accepted 9 May 1995)

In a series of spectroscopic work of the Rydberg states of CO, we present the rotational analysis of the $v=0$ and 1 levels of the singlet ns, np, nd and nf-Rydberg states ($n=4$–7). The spectra were measured by ion-dip spectroscopy with triple resonance excitation via the $3s\sigma{:}B\ ^1\Sigma^+$ or the $3p\sigma{:}C\ ^1\Sigma^+$ state. All the spectra were rotationally well resolved and the term value, quantum defect and the rotational constant were obtained for each state. Through the analysis of the rotational structure, the coupling between the Rydberg electron and the ion core has been investigated. For the np-Rydberg states, a switching from Hund's case (b) to (d) was clearly observed with the increase of n. A significant perturbation was observed in the $6p\pi\ ^1\Pi$ and $7p\pi\ ^1\Pi$ states and it is suggested that these states are perturbed by the state with the same symmetry. For the nf-Rydberg states, the observed electronic energy was well analyzed by the long range force model and the precise ionization potential was obtained. The Rydberg↔valence and inter-Rydberg states interactions were also investigated. For the ns-Rydberg states, the interaction matrix element with the repulsive state was estimated from the measurement of linewidth of the rotational levels. The potential curve of the repulsive state to which ns-Rydberg states predissociate was also determined. Selective predissociation was found for the e-symmetry levels both in the $v=0$ and 1 levels of the nf-Rydberg state. A strong interaction between the $v=0$ levels of the $6d$- and $7s$-Rydberg states was observed. © *1995 American Institute of Physics.*

I. INTRODUCTION

Carbon monoxide (CO) is the secondary most abundant molecules after H_2 in the interstellar medium. Because of the importance of the dissociation in the vacuum ultraviolet region, the absorption spectrum and the dissociation have been extensively studied in the region of 90–115 nm.[1–7] Letzelter *et al.* measured the absorption cross section and obtained the dissociation yield.[1] They concluded that the photodissociation of CO proceeds after the excitation to discrete states. In this energy region, most of the discrete states are the Rydberg states and therefore the investigation of energy levels, absorption cross sections and the interactions with valence states are of special importance. Especially, it is thought that the $D'\ ^1\Sigma^+$ valence state play an important role for the dissociation of the high Rydberg states.[8,9] In *ab initio* calculations, the $3s\sigma{:}B\ ^1\Sigma^+$ and D' states are strongly coupled with each other, resulting in a double minimum adiabatic state (BD').[8] Tchang-Brillet *et al.* calculated the $B\ ^1\Sigma^+$–$D'\ ^1\Sigma^+$ homogeneous interaction in detail by the close coupling method and obtained the potential curve of the D' state in the region close to the B state.[9] However, the interaction in the higher Rydberg states has not been investigated yet. Especially, it is very important to investigate the Rydberg-D' interaction in the region of 100 000–110 000 cm^{-1}, since the interaction causes the predissociation.

Many experiments based on one-photon absorption spectroscopy have been performed to analyze the rotational structure and to determine the absorption cross section.[1–5] Eidelsberg *et al.* observed the high resolution absorption spectra of four isotopic species of CO.[3–5] Also many laser spectroscopic measurements have been extensively performed. Optogalvanic spectroscopy has been applied to measure the inter-Rydberg transitions.[10–13] Four wave mixing spectroscopy[14,15] and different resonantly enhanced multiphoton schemes have been applied.[16–18] Recently, high resolution spectroscopy was performed by using an extreme-ultraviolet laser source with narrow band,[19–21] and by fluorescence depletion method.[22] Our group reported the triple-resonant spectroscopic study of the Rydberg states.[23–25] In this spectroscopy, CO molecules are first pumped to the well known lower Rydberg states, such as the $3s\sigma B\ ^1\Sigma^+$ or $3p\sigma C\ ^1\Sigma^+$ state, by two-color double resonance excitation and the third laser pumps the excited CO molecules to the higher Rydberg states. Since we measure the spectrum from a single rotational level of the $B\ ^1\Sigma^+(C\ ^1\Sigma^+)$ state and the inter-Rydberg transition favors the $\Delta v=0$ propensity, the higher Rydberg←$B(C)$ absorption spectrum is greatly simplified. In our previous papers, we measured the $v=1$ level of the ns, np, nd, and nf-Rydberg states for $n\geqslant 4$ in the energy region of 108 000–115 000 cm^{-1} and analyzed their rotational structure. Term values and rotational constants were obtained for each state. Through the detailed analysis of the rotational structures, many interaction such as Rydberg–Rydberg and Rydberg-valence interactions were investigated. It was found that the e-symmetry component of the nf-Rydberg states predissociates much faster than the f-symmetry component and it was suggested that the nf-Rydberg state predissociates through the D' valence state.[25]

In the present paper, we report the extended study to the $v=0$ level of the Rydberg states and describe a comparison with the $v=1$ level. Figure 1 shows the energy diagram of the Rydberg states whose rotational structures have been analyzed already or analyzed in the present experiment. In this work, the analyses of four Rydberg series, ns, np, nd, and

 0021-9606/95/103(7)/2420/16/$6.00

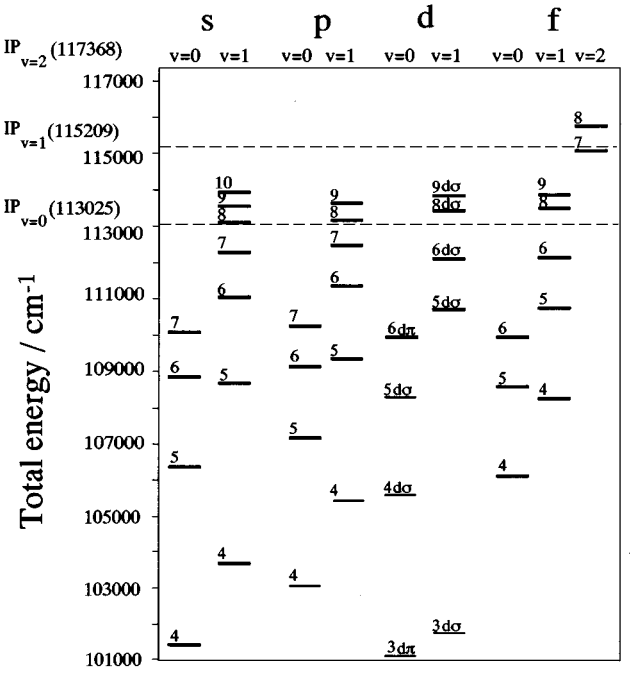

FIG. 1. Energy level diagram of the Rydberg states of CO whose rotational structures were analyzed. Thick solid lines indicate the states which were analyzed with triple resonant spectroscopy.

nf with $n=4-7$ and $v=0$ are presented. For the $4s-6s$-Rydberg states, the interaction with the repulsive state and their predissociation were investigated by the measurement of the linewidth. The interaction between the Rydberg electron and the ion core was investigated on the basis of l-uncoupling model for the np and the nf-Rydberg states. The interaction between the nd-Rydberg and the $(n+1)s$-Rydberg state is also discussed.

II. EXPERIMENT

The experimental setup for ion-dip spectroscopy with triple resonant excitation was described in a previous paper.[25] Briefly, jet-cooled CO was excited to a single rovibrational level ($v''=0$ and 1, J'') of the $3s\sigma B\ ^1\Sigma^+$ or the $3p\sigma C\ ^1\Sigma^+$ state by double resonant excitation through the $A\ ^1\Pi$ $(v=4)$ state with two laser beams (ν_1,ν_2). Part of the CO molecules excited to the $B(C)$ state are further ionized by absorbing additional photons of ν_1 or ν_2. This ion signal is used for monitoring the CO population in the B (or C) state. Third laser (ν_3) is introduced to excite CO in the B state to the higher Rydberg states. Since most of the Rydberg states are predissociative, the CO molecules excited to the Rydberg states immediately dissociate, leading in a depletion of the ion signal. Therefore, by scanning the third laser frequency while monitoring the ion signal, the ion-dip spectrum is obtained, representing the transition to the high Rydberg from the $B(C)$ state.

The three dye lasers (one Lambda Physik FL2002 and two Molectron DL14) were simultaneously pumped by a XeCl excimer laser (Lambda Physik EMG 103 MSC). The second harmonics of the dye laser (FL2002) was used as ν_1 for the two-photon excitation of CO to the $A\ ^1\Pi(v=4)$ state. Typical ν_1 laser pulse energy was 300 μJ. The second dye laser (DL 14) was used as ν_2 for the $B\ ^1\Sigma^+-A\ ^1\Pi(v=4)$ transition and its typical power was 4μJ. Both the laser beams were introduced coaxially in the same direction into a vacuum chamber. The output of the third dye laser, ν_3, was counterpropagated to the two laser beams. The three laser beams were focused by $f=250$ mm lenses 15 mm downstream of a pulsed nozzle. Pure CO gas was expanded into the vacuum chamber through the nozzle having a 400 μm orifice. The generated ions by the REMPI were repelled by an electric field of 4 V/cm and detected by an electron multiplier (Murata Ceratron). The ion signal was amplified and integrated by a boxcar integrator (Par 4400/4420) connected with a personal computer. Though the frequency of the three dye lasers were calibrated by a calibrated double monochromator and their accuracy was 1 cm^{-1}, the rotational energy levels of the B (and C) was adopted from those obtained by absorption spectrum.[3,26]

III. RESULTS AND DISCUSSION

A. $4s\sigma$, $5s\sigma$, and $6s\sigma$ Rydberg states ($v=0$ and 1)

In the previous paper, the rotational analyses of the $v=1$ level of the ns-Rydberg states with $n\geqslant 5$ were reported. The rotational analysis of the $v=0$ level has been presented only for a few states. For the $4s\sigma(v=0)$ state, Ogawa and Ogawa obtained the term value T_e from the rotationally unresolved spectrum.[6,7] Very recently, the $4-6s\sigma(v=0)$ states were reinvestigated and the rotational structure of the $6s\sigma(v=0)$ state was analyzed by Eidelsberg *et al.*[4] However, they mentioned that the absorption spectra of the (0-0) bands of the $4s\sigma\ ^1\Sigma^+$ and $5s\sigma\ ^1\Sigma^+$ states were diffuse and the rotational structures were not analyzed. In the present experiment, the rotational structures of the $4s\sigma-7s\sigma$ states $(v=0)$ were clearly resolved, demonstrating the ability of triple resonant ion-dip spectroscopy.

Figure 2 shows the triple resonant ion-dip spectrum of the $4s\sigma\ ^1\Sigma^+(v'=0,J')\leftarrow B\ ^1\Sigma^+$ $(v''=0,\ J''=0-4)$ transition. The ν_3 frequency is in the range of 14 450–14 650 cm^{-1}, which corresponds to the total energy of 101 370–101 570 cm^{-1}. As can be seen in the figure, a single dip at $J''=0$ and two dips at $J''\geqslant 1$ are observed for the $4s\sigma\ ^1\Sigma^+(v'=0)\leftarrow B\ ^1\Sigma^+(v''=0)$ transition and no other transition is seen in this energy region. These dips are easily assigned to the P and R branches characteristic to the $^1\Sigma^+\leftarrow{}^1\Sigma^+$ transition. The total energy of the rotational levels of $4s\sigma(v=0)$ is obtained by adding the observed ν_3 frequency to the energy of the $B\ ^1\Sigma^+(v=0)$ intermediate state. Straight line was obtained by plotting total energy level against $J(J+1)$ and the term value (T_Σ) and the rotational constant (B) for the $4s\sigma\ ^1\Sigma^+(v=0)$ state were obtained to be 101 454 cm^{-1} and 2.0 cm^{-1}, respectively, which are listed in Table I. As is seen in the table, the term value is in a good agreement with the value reported by Ogawa and Ogawa,[6,7] which was obtained from the rotationally unresolved absorption spectrum. Another important point in the spectrum is the broadness of the rotational lines. The rotational linewidth of the spectrum shown in Fig. 2 is as large as 17 cm^{-1}, which was independent of J within the experimental error limit.

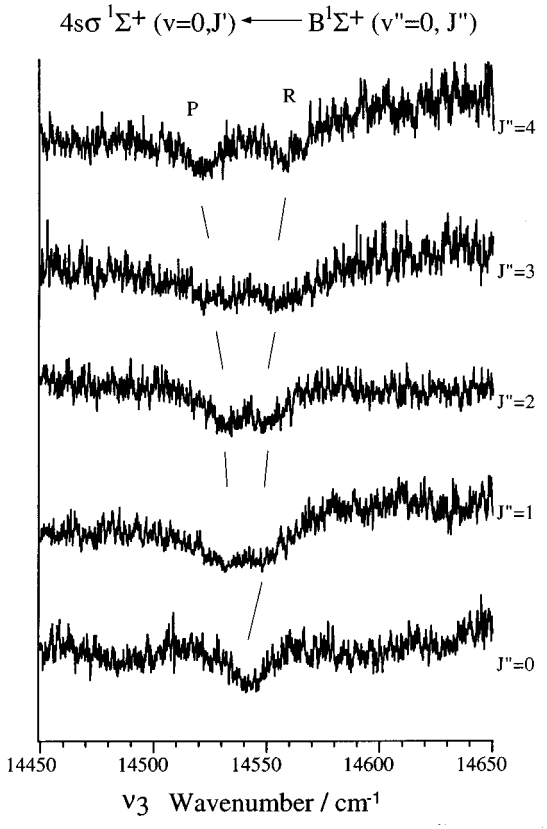

FIG. 2. Triple resonant ion-dip spectra of CO showing the $4s\sigma\ ^1\Sigma^+(v=0,J')\leftarrow B\ ^1\Sigma^+(v=0,J'')$ transition.

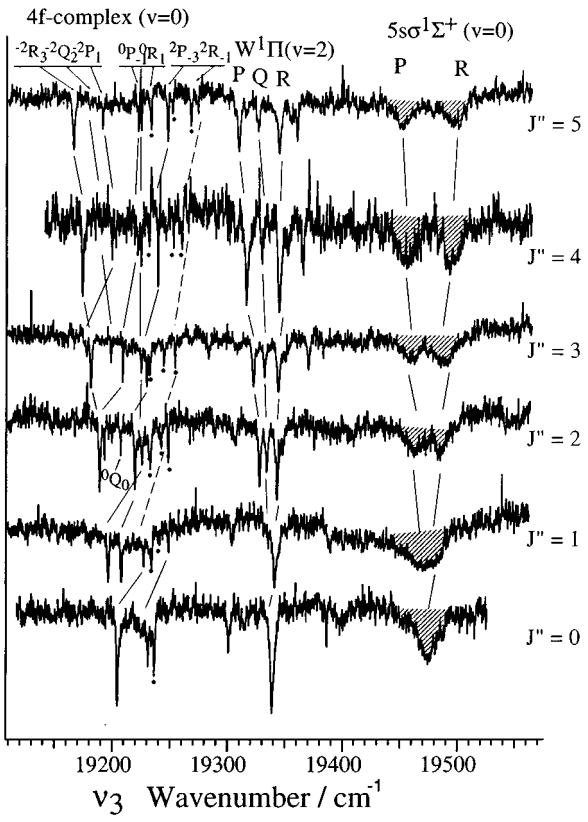

FIG. 3. Triple resonant ion-dip spectra of CO showing the $4f(v=0,J')$, $W\ ^1\Pi(v=2,J')$, and $5s\sigma\ ^1\Sigma^+(v=0,J')\leftarrow B\ ^1\Sigma^+(v=0,J'')$ transitions.

The broadness is due to the fast predissociation to a repulsive state. The interaction between the $ns\sigma$-Rydberg and the repulsive valence state will be discussed later.

The ion-dip spectra of the $5s\sigma\ ^1\Sigma^+(v'=0,J')\leftarrow B\ ^1\Sigma^+(v''=0,J'')$ transition is observed at $\nu_3\sim 19\,470\ \mathrm{cm}^{-1}$ in Fig. 3. Though the rotational lines are well resolved, they are also broad as was seen in the $4s\sigma(v=0)\leftarrow B\ ^1\Sigma^+(v''=0)$ spectra. The rotational energy levels of the $5s\sigma(v=0)$ state are plotted in Fig. 4, from which the values of $T_\Sigma=106\,386\ \mathrm{cm}^{-1}$, $\delta=0.934$, and $B=2.01\ \mathrm{cm}^{-1}$ were obtained for $5s\sigma(v=0)$. T_Σ of $5s\sigma(v=0)$ agrees well with the value reported by Stark *et al.*[2] The rotational constant of $5s\sigma(v=0)$ is slightly larger than that of the ion core ($1.9772\ \mathrm{cm}^{-1}$).[27]

Figure 5 shows the ion-dip spectra of the $6s\sigma(v'=0,J')\leftarrow B\ ^1\Sigma^+(v''=0,J'')$ transition together with

TABLE I. Term value (T_Σ), rotational constant (B), quantum defect (δ), vibrational energy spacing between $v=0$ and 1 (ΔG), and difference (δG) of ΔG of the $ns\sigma$ Rydberg states from that of CO^+.[a]

							Previous values[b]	
$ns\sigma$	v	T_Σ (cm^{-1})	B (cm^{-1})	δ	ΔG (cm^{-1})	δG (cm^{-1})	T_Σ (cm^{-1})	B (cm^{-1})
$3s\sigma$[c]	0	86 916.18	1.948 18	0.950			86 916.18[c]	1.948 18[c]
	1	88 998.32	1.921 90	0.954	2082	−102	88 998.32[c]	1.921 90[c]
$4s\sigma$	0	101 454	2.00	0.920			101 456[d]	⋯
	1	103 691	1.92	0.913	2237	+53	103 691.3[d]	1.920 3[d]
$5s\sigma$	0	106 386	2.01	0.934			106 383[e]	⋯
	1	108 678	1.89	0.901	2292	+108	108 678.0[c]	1.905 0[c]
$6s\sigma$	0	108 793	2.14	0.908			108 788[c]	2.14[c]
	1	111 028	2.01	0.877	2235	+51	⋯	⋯
$7s\sigma$	0	110 049	1.30	0.928			⋯	⋯
	1	112 275	2.15	0.884	2226	+42	⋯	⋯

[a]$CO^+\ X\ ^2\Sigma^+$; $\Delta G^i=2184\ \mathrm{cm}^{-1}$.
[b]These values were obtained by the one-photon absorption spectra.
[c]Reference 4.
[d]Reference 6.
[e]Reference 37.

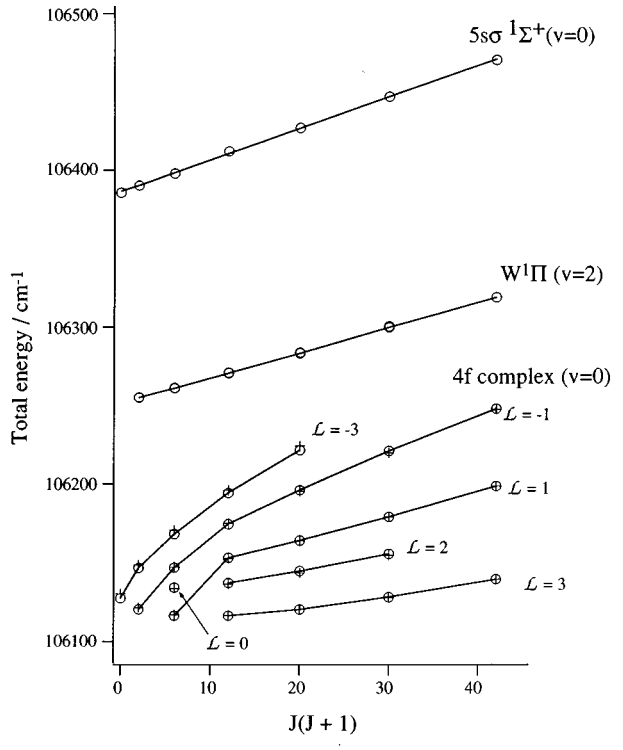

FIG. 4. Plot of the energy levels of the $4f(v=0)$, $W\ ^1\Pi(v=2)$, and $5s\sigma\ ^1\Sigma^+(v=0)$ states vs $J(J+1)$. ○, Observed levels; +, calculated energy levels obtained by *l*-uncoupling model (see text).

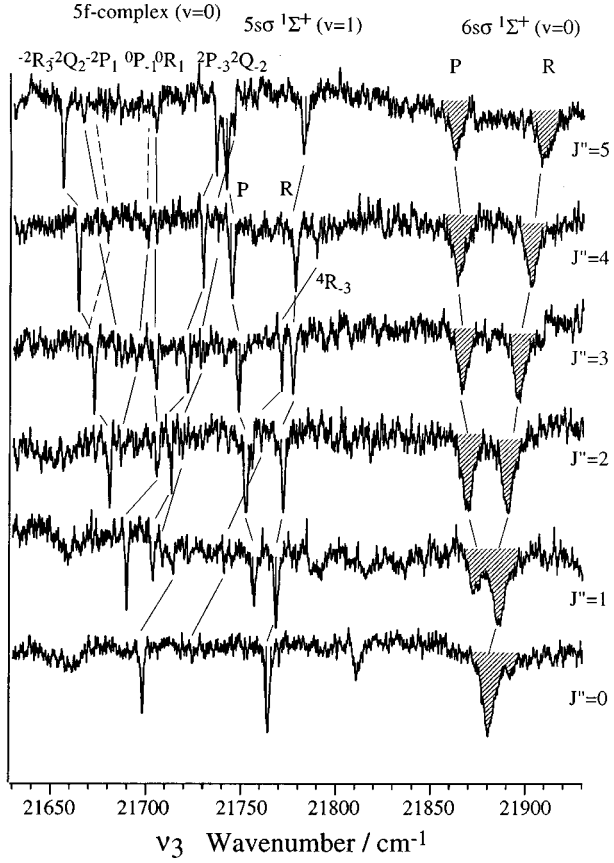

FIG. 5. Triple resonant ion-dip spectra of CO showing the $5f(v=0,J')$, $5s\sigma\ ^1\Sigma^+(v=1,J')$ and $6s\sigma\ ^1\Sigma^+(v=0,J')\leftarrow B\ ^1\Sigma^+(v=0,J'')$ transitions.

other transitions. *P* and *R* branches of the $6s\sigma\ ^1\Sigma^+\leftarrow B\ ^1\Sigma^+$ transition are easily identified at $\nu_3\sim 21\,880\ \mathrm{cm}^{-1}$ and the plot of energy levels vs $J(J+1)$ is shown in Fig. 6. For $6s\sigma(v=0)$, $T_\Sigma=108\,793\ \mathrm{cm}^{-1}$, $\delta=0.908$, and $B=2.14\ \mathrm{cm}^{-1}$ are obtained. The rotational constant of $6s\sigma(v=0)$ agrees well with that reported by Eidelsberg *et al.*[4] and it is larger than that of the ion core. The linewidth of $6s\sigma(v=0)$ is $3.8\ \mathrm{cm}^{-1}$, which is narrower than the linewidth of $4s\sigma(v=0)$ and $5s\sigma(v=0)$. This indicates that the predissociation rate of $6s\sigma(v=0)$ is slower than $4s\sigma(v=0)$ and $5s\sigma(v=0)$.

From the values of T_Σ for $v=0$ and those for $v=1$ previously obtained, the energy difference, ΔG,

$$\Delta G=T_\Sigma(v=1)-T_\Sigma(v=0), \tag{1}$$

was obtained for each *ns* state. We introduce the following value, δG, which represents the difference from ΔG of the CO^+ ion;

$$\delta G=\Delta G-\Delta G^i. \tag{2}$$

Here ΔG^i $(=2184\ \mathrm{cm}^{-1})$ is ΔG of CO^+ in the ground state and δG is related to the distortion of the potential curve of the Rydberg state from that of the ion core. The obtained ΔG and δG are also listed in Table I. As can be seen in Table I, ΔG of the $4-6s\sigma$ states are larger than that of the ion core. On the other hand, δG of $3s\sigma{:}B\ ^1\Sigma^+$, the lowest member of the $ns\sigma$ state, is $-102\ \mathrm{cm}^{-1}$. The potential distortion is thought to occur by the interaction with the repulsive state, such as the $D'\ ^1\Sigma^+$ valence state. For the $B\ ^1\Sigma^+$ state, Tchang-Brillet *et al.* calculated the interaction with the D' state by using two-state diabatic model.[9] For the $B\ ^1\Sigma^+$ state, the D' potential curve crosses at the bond length longer than the equilibrium position of the *B* state. On the other hand, the positive δG values for the $n\geqslant 4$ states indicate that the repulsive potential curve crosses at their equilibrium bond length or at even shorter position.

The potential curve distortion of the $ns\sigma$-Rydberg states is also recognized in the transition intensity of the Rydberg $(v')\leftarrow 3s\sigma B\ ^1\Sigma^+(v''=0)$ ion-dip spectrum. Though Rydberg–Rydberg transitions are usually governed by a strong $\Delta v=0$ propensity, we found that the $\Delta v\neq 0$ transition also occurs in the $ns\sigma\ ^1\Sigma^+(v')\leftarrow 3s\sigma B\ ^1\Sigma^+(v'')$ transition. For example, in Fig. 5, the $5s\sigma\ ^1\Sigma^+(v'=1)\leftarrow 3s\sigma B\ ^1\Sigma^+(v''=0)$ transition is clearly observed at lower frequency side of the $6s\sigma\ ^1\Sigma^+(v'=0)\leftarrow 3s\sigma B\ ^1\Sigma^+(v'')$ transition. We found that the similar $\Delta v\neq 0$ transition is also observed in the spectrum reported in the previous paper;[28] weak dips due to the $6s\sigma\ ^1\Sigma^+(v'=0)\leftarrow 3s\sigma B\ ^1\Sigma^+(v''=1)$ transition are observed at $110\ \mathrm{cm}^{-1}$ higher frequency side of the $5s\sigma(v=1)\leftarrow 3s\sigma B\ ^1\Sigma^+(v''=1)$ transition. These $\Delta v\neq 0$ transitions are thought to occur due to the potential curve distortion of the $ns\sigma$ states by the perturbation of the repulsive state. In the next two sections, we will discuss the interaction between the $ns\sigma$ state and the repulsive state from the observed rotational linewidth and its dependence on principal quantum number and on vibrational level.

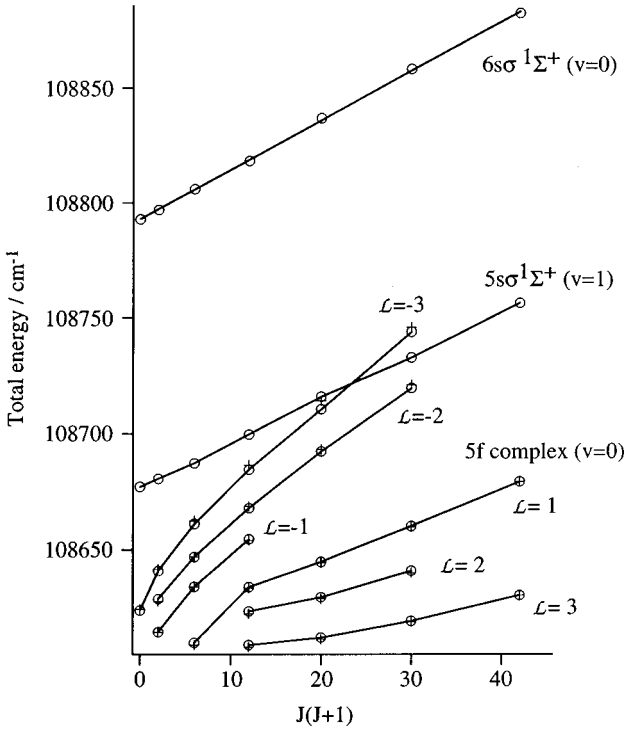

FIG. 6. Plot of the energy levels of the $5f(v=0)$, $5s\sigma\ ^1\Sigma^+(v=1)$ and $6s\sigma\ ^1\Sigma^+(v=0)$ states vs $J(J+1)$. ○, Observed levels; +, calculated energy levels obtained by *l*-uncoupling model.

B. Linewidth of the $4s\sigma-6s\sigma(v=0$ and 1) Rydberg states

As was pointed previously, the rotational linewidth of the $ns\sigma(v=0)$ state depends on n. We should also point out that we did not see the rotational level (J) dependence on the other hand. Since the broadening of the $ns\sigma$ states occurs due to the predissociation to the repulsive state, the interaction matrix element and the potential curve of the repulsive state can be obtained from the analysis of the linewidth. In the ion-dip spectrum, however, a careful examination is necessary to obtain the true linewidth, Γ, because the dip is often broadened by the saturation effect due to an intense laser pulse energy, which was described in the previous paper.[25] In this section we discuss the quantitative estimation of the linewidth of the Rydberg states.

Very recently, the fluorescence dip spectra of the Rydberg$\leftarrow B\ ^1\Sigma^+(v''=0)$ transitions of CO were reported by Drabbels *et al.*[22] In the fluorescence dip spectrum, they estimated the linewidth by using the two-level scheme. In the present paper, we also used the two-level scheme of the B and high Rydberg states. The difference between the fluorescence-dip and the ion-dip methods is whether one measures the fluorescence intensity or ionization intensity to monitor the B state population. Figure 7 shows the excitation schemes in the case whether ν_3 is resonant (ν_3 on) to the high Rydberg state or is not resonant (off), respectively. In the present experimental condition, the ionization of the B state molecules occurs mainly by ν_1. Therefore, in the case that ν_3 is not resonant to the transition (off-resonant, case a), the B state molecules are ionized by ν_1 or decay with the rate of k_T. In this case, the rate equation is given by

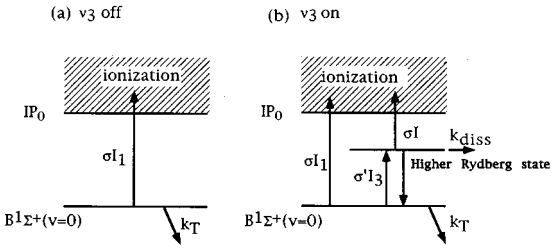

FIG. 7. Excitation scheme used to calculate the relative absorption cross section of the high Rydberg$\leftarrow B\ ^1\Sigma^+$ transition. k_T is the total decay rate of the B state. $k_{\rm diss}$ is the predissociation rate of the B state. σ is the ionization cross section and σ' is the Rydberg$\leftarrow B$ absorption cross section. I_1 and I_3 are the ν_1 and ν_3 laser powers and $I(=I_1+I_2+I_3)$ is the total laser powers.

$$d[B]/dt=-(k_T+\sigma I_1)[B]. \tag{3}$$

Here, $[B]$ is the time dependent population in the B state, σ is the ionization cross section of the B state, and I_1 is the ν_1 power in unit of cm^{-2} s^{-1}. Then the total ion intensity is given by

$$[\mathrm{ion}]_{\rm off}=\int_0^t\{\sigma I_1[B]\}dt=\frac{\sigma I_1[B]_0}{k_T+\sigma I_1}\times\{1-\exp[-(k_T+\sigma I_1)t]\}. \tag{4}$$

Here, $[\mathrm{ion}]_{\rm off}$ is the total ion intensity in the case that ν_3 is off-resonant, $[B]_0$ is the initial population in the B state, and t is the ν_3 laser irradiation time, respectively.

In the case that ν_3 is resonant to the Rydberg state (case b), the rate equations are given by

$$d[B]/dt=-(k_T+\sigma I_1+\sigma' I_3)[B]+\sigma' I_3[R], \tag{5a}$$

$$d[R]/dt=\sigma' I_3[B]-(\sigma' I_3+\sigma I+k_{\rm diss})[R]. \tag{5b}$$

Here $[R]$ is the population in the Rydberg state, σ' is the cross section of the Rydberg$\leftarrow B$ transition, $k_{\rm diss}$ is the predissociation rate of the Rydberg state. We assumed that $k_{\rm diss}$ is much larger than the radiative decay rate, which is reasonable because none of the Rydberg states with $n\geqslant 4$ emits fluorescence. I_3 is the power of ν_3 and I is the total $(I=I_1+I_2+I_3)$ power in unit of cm^{-2} s^{-1}. In Eq. (5), ν_3 contributes to both absorption and stimulated emission between the B and Rydberg states. The decay of the Rydberg state molecules is governed by the predissociation and the ionization. In this case, the total ion intensity is given by

$$[\mathrm{ion}]_{\rm on}=\int_0^t\{\sigma I_1[B]+\sigma I[R]\}dt=\frac{\sigma I_1[B]_0\{a+2\sigma' I_3-\sqrt{c^2+(2\sigma' I_3)^2}\}}{2(a\sigma' I+b)}\times(1-\exp\{-[a+2\sigma' I_3+\sqrt{c^2+(2\sigma' I_3)^2}]t/2\}), \tag{6}$$

where

$$a=(k_T+\sigma I_1)+(k_{\text{diss}}+\sigma I),$$
$$b=(k_T+\sigma I_1)\times(k_{\text{diss}}+\sigma I), \tag{7}$$
$$c=(k_T+\sigma I_1)-(k_{\text{diss}}+\sigma I).$$

Here $[\text{ion}]_{\text{on}}$ is the total ion intensity when ν_3 is resonant to the Rydberg state. When the ν_3 power is zero ($I_3=0$), $[\text{ion}]_{\text{on}}=[\text{ion}]_{\text{off}}$ in Eq. (6). When $I_3\neq 0$, the depletion is obtained by comparing $[\text{ion}]_{\text{on}}$ with $[\text{ion}]_{\text{off}}$. We first introduce the ionization ratio, $R(=[\text{ion}]_{\text{on}}/[\text{ion}]_{\text{off}})$, which represents the ion-dip spectrum. In the calculation, R was calculated as a function of I_3 for given values of k_{diss}. For the calculation, the ionization cross section was set to 10^{-18} cm^2, which was adopted from the ionization cross section of the A state of NO,[29] while the Rydberg$\leftarrow B$ transition cross section was set to 10^{-16} cm^2. The decay rate of the B state of CO (Ref. 22) is reported to be 3.3×10^7 s^{-1}. The photon density of the ν_1 laser was set to 3×10^{25} cm^{-2} s^{-1}, which was estimated from the laser pulse energy, pulse length (10 ns), and the beam waist at the focusing point. The photon density of the ν_2 laser was set to 4×10^{23} cm^{-2} s^{-1} and that of ν_3 was varied from 4×10^{23} cm^{-2} s^{-1} to 4×10^{24} cm^{-2} s^{-1}. We found that for a given value of σ, R becomes constant when k_{diss} is equal to or larger than 10^{11} s^{-1} under the same I_3. Therefore, R becomes independent of k_{diss} when $k_{\text{diss}}\geqslant 10^{11}$ s^{-1}. This result agrees with the relationship between the linewidth and the fluorescence depletion given by Drabbels *et al.*[22] In the high Rydberg states of CO, the predissociation rate is equal to or larger than the order of 10^{11} s^{-1} and therefore the relation of $k_{\text{diss}}\gg k_T$, $\sigma' I_3$, and σI is a reasonable assumption in the present experimental condition. Then, the terms in Eq. (7) is simplified to $a=k_{\text{diss}}$, $b=(k_T+\sigma I_1)\times k_{\text{diss}}$, and $c=-k_{\text{diss}}$. From Eqs. (4) and (7), R is given by

$$R=[\text{ion}]_{\text{on}}/[\text{ion}]_{\text{off}}=k_T/(\sigma' I_3+k_T), \tag{8}$$

which depends simply on $\sigma' I_3$ and k_T. To evaluate the absorption cross section σ' of the Rydberg$\leftarrow B$ transition, we next introduce the inverse ionization ratio,

$$R^{-1}=[\text{ion}]_{\text{off}}/[\text{ion}]_{\text{on}}=(\sigma'/k_T)\times I_3+1, \tag{9}$$

which linearly increases with I_3 when the Rydberg state is predissociative. To confirm this relationship, we measured the I_3 dependence of R^{-1} under the condition that the Rydberg$\leftarrow B$ transition is not saturated.

Figure 8 shows the plot of R^{-1} of the $5s\sigma(v=0)\leftarrow B\ ^1\Sigma^+(v=0)$ transition against I_3. As is seen in the figure, the linear dependence is obtained and the intersect is equal to 1, which agrees with Eq. (9). From Eq. (9), we may obtain the absolute absorption cross section, σ', if we know the values of k_T and I_3. However, an accurate estimation of the laser pulse energy at the ion-dip region is very difficult, so we obtained the relative value of σ' instead. Therefore, R^{-1} spectrum corresponds to the relative Rydberg$\leftarrow B$ absorption spectrum and the linewidth can be obtained from the spectrum.

In Figs. 9(a) and 9(b) are plotted the R and the R^{-1} spectra of the $5s\sigma(v=0)$, $W\ ^1\Pi(v=2)$, and $4f(v=0)\leftarrow B\ ^1\Sigma^+$ $(v=0, J''=0)$ transitions. The lifetime of the $W\ ^1\Pi(v=2)$ state was recently obtained to be

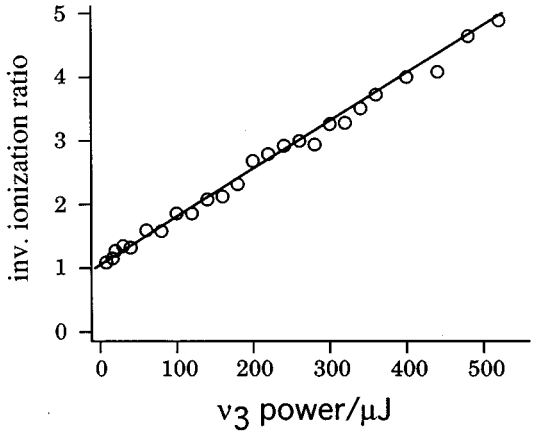

FIG. 8. Plot of the inverse ionization ratio, R^{-1}, vs ν_3 laser power for the $5s\sigma(v=0)\leftarrow B\ ^1\Sigma^+(v=0)$ transition.

8.3×10^{-10} s.[21] Therefore, Eqs. (9) and (10) are also applicable for the $W\ ^1\Pi(v=2)$ state. The linewidth Γ(FWHM) for the $W\ ^1\Pi(v=2)$ and $5s\sigma(v=0)$ states obtained from the R^{-1} spectrum was 1 cm^{-1} and 15 cm^{-1}, respectively. The lifetime, τ, is deduced from the width Γ by

$$\tau=k^{-1}=1/(2\pi\Gamma c). \tag{10}$$

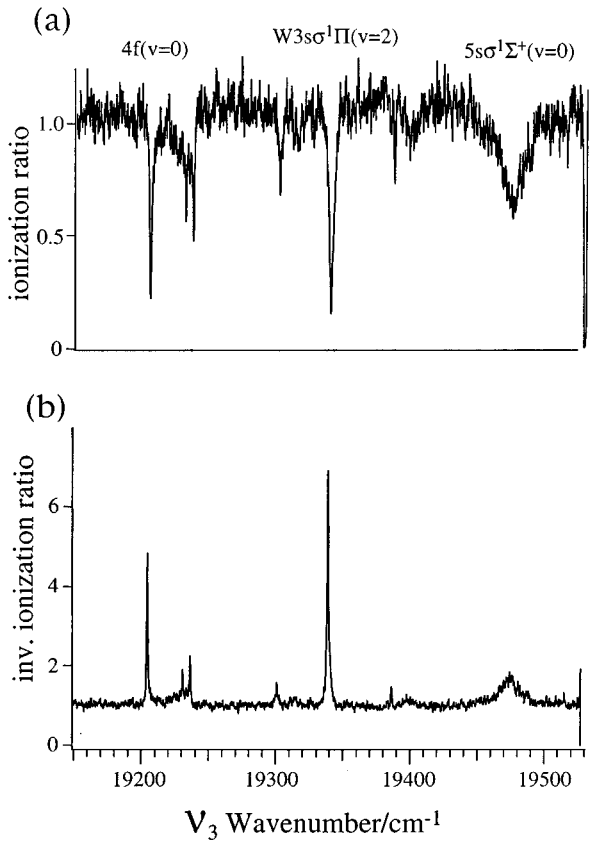

FIG. 9. (a) Ionization ratio (R) spectrum and (b) Inverse ionization ratio (R^{-1}) spectrum of the $4f(v=0)$, $W\ ^1\Pi(v=2)$ and $5s\sigma(v=0)\leftarrow B(v=0,J''=0)$ transitions.

Here, c is the speed of light. Since the linewidth of the ν_3 laser is 1 cm^{-1}, the lifetime of the $W\ ^1\Pi(v=2)$ state was obtained as a maximum value to be 5.3×10^{-12} s and the predissociation rate to be smaller than 1.9×10^{11} s^{-1}. The lifetime and the predissociation rate of $5s\sigma$ were obtained to be 0.35×10^{-12} s and 2.8×10^{12} s^{-1}, respectively. It should be noted that this is the value of the single rotational line and therefore it is more accurate than the value estimated from the absorption spectrum in which many rotational lines are overlapped.

By the same procedure, the values of Γ of other $ns\sigma$ Rydberg states were obtained. Figure 10 shows the R^{-1} spectra of the $4-6s\sigma(v'=0$ and 1, $J'=1)\leftarrow B\ ^1\Sigma^+(v=0$ and 1, $J''=0)$ transitions. It is clear that the linewidth depends on not only the principal quantum number but also on the vibrational level. The linewidth of $4s\sigma(v=0)$ is almost same as that of $5s\sigma(v=0)$, while the linewidth of $6s\sigma(v=0)$ is narrower. On the other hand, all the rotational lines become narrower at $v=1$. Obtained values of Γ and lifetimes for the $4s\sigma-6s\sigma(v=0$ and 1) states are listed in Table II.

C. Interaction between $4-6s\sigma$ and repulsive valence state

The line broadening observed for the $ns\sigma$-Rydberg states occurs due to the predissociation to the repulsive valence state. Among the several repulsive states, the $D'\ ^1\Sigma^+$ state has been believed to be responsible for the predissociation of the $ns\sigma$-Rydberg states.[4] As seen in the previous section, the linewidth depends significantly on the principal quantum number and on vibrational level. Therefore, we calculated the interaction matrix element from the observed linewidth and investigated the repulsive potential curve to which CO in the Rydberg state predissociates. The interaction between the bound ($ns\sigma$-Rydberg) and the continuum states is determined by[30]

$$H_{v,J;E,J}=\langle\Psi_{1,v,J}|\mathbf{H}|\Psi_{2,E,J}\rangle$$
$$=\langle\phi_1(r,R)\chi_{v,J}(R)|\mathbf{H}|\phi_2(r,R)\chi_{E,J}(R)\rangle. \quad (11)$$

Here $H_{v,J;E,J}$ is the interaction matrix element and $\mathbf{H}$ is the coupling operator for predissociation. $\Psi_{1,v,J}$ and $\Psi_{2,E,J}$ are the total wave functions, $\phi_1(r,R)$ and $\phi_2(r,R)$ are the electronic wave functions, and $\chi_{v,J}(R)$ and $\chi_{E,J}(R)$ are the eigenfunctions in the bound and continuum states, respectively, where $\chi_{E,J}(R)$ is energy-normalized. In the diabatic representation, the electronic matrix element is independent of R, or varies linearly with R. And the matrix element $H_{v,J;E,J}$ is separated into two parts,

$$H_{v,J;E,J}=\langle\phi_1(r,R)|\mathbf{H}|\phi_2(r,R)\rangle\langle\chi_{v,J}(R)|\chi_{E,J}(R)\rangle$$
$$=H^e\langle\chi_{v,J}(R)|\chi_{E,J}(R)\rangle. \quad (12)$$

The linewidth (Γ) can be expressed by the Fermi Golden Rule formula and from Eq. (12) it is given as,

$$\Gamma_{v,J}=2\pi|H_{v,J;E,J}|^2=2\pi|H^e|^2|\langle\chi_{v,J}(R)|\chi_{E,J}(R)\rangle|^2, \quad (13)$$

where $|\langle\chi_{v,J}(R)|\chi_{E,J}(R)\rangle|^2$ is the differential Franck–Condon factor with the E^{-1} dimension (cm). In Eq. (13), H^e varies slowly with energy. If H^e is assumed to be constant in a given electronic state, the variation of Γ with v is governed by the differential Franck–Condon factor. We applied the diabatic representation Eq. (12) to the interaction between the $4-6s\sigma$ $(v=0,1)$ states and the repulsive state. From Eq. (13), the ratio of Γ of $v=0$ to that of $v=1$ in the given electronic state is equal to the ratio of $|\langle\chi_{v,J}(R)|\chi_{E,J}(R)\rangle|^2$, that is

$$\frac{\Gamma(v=1)}{\Gamma(v=0)}=\frac{|\langle\chi_{1,J}(R)|\chi_{E',J}(R)\rangle|^2}{|\langle\chi_{0,J}(R)|\chi_{E'',J}(R)\rangle|^2} \quad (14)$$

with the assumption of the invariant H^e in the state. In the calculation, the potential curves of the $4-6s\sigma$ states were assumed to be the same with that of the ion core ($\omega_e=2214.2$ cm^{-1}, $\omega_e x_e=15.16$ cm^{-1}, and $r_e=1.115$ Å). The potential curve of the repulsive state was assumed to be expressed by an exponential function. The wave functions, $\chi_{v,J}(R)$, $\chi_{E,J}(R)$, were calculated by using a numerical integration method. Energy normalization of the continuum wave function was performed so that their asymptotic amplitudes are normalized to $0.2788(\mu/E)^{1/4}$ in units of cm^{-1} Å, where μ is the reduced mass of CO in amu and E is the asymptotic kinetic energy in unit of cm^{-1}.[31] Parameter fitting of the function was carried out so as to reproduce the observed ratio between $v=0$ and 1 for the $4s\sigma-6s\sigma$ states. The best result was obtained when the repulsive potential curve is expressed as $V(R)=2.761\times10^9\exp(-10.8R)$ in unit of cm^{-1}. The relative energy between the bottom of the $4s\sigma$ potential curve and the asymptotic value of the repulsive state was set to be 10 759 cm^{-1}. The calculated differential Franck–Condon factors are listed in Table II and Fig. 11 shows the diabatic potential curves obtained for the repulsive state and the $4-6s\sigma$ states in the energy region from 9 800 to 11 200 cm^{-1}.

As is seen in Fig. 11, the potential curve of the repulsive state crosses near the bottoms of the $4s\sigma$ and $5s\sigma$ potential curves. Therefore, the Franck–Condon factor significantly changes from $v=0$ to 1, which is in good agreement with the observed vibrational dependency of Γ of the two states. On the other hand, the repulsive potential curve crosses at the inner position of the $6s\sigma$ potential curve and the vibrational dependence of Γ is rather small, which also agrees well with the observed result.

It is not clear whether the repulsive state investigated in the present work is the D' state or not. The D' state potential curve at the lower energy region was obtained by Tchang-Brillet *et al.* from the analysis of the $B-D'$ interaction. We also calculated the Franck–Condon factors between the $4s-6s\sigma$ states and the D' state reported by them and the results are listed in Table II. As seen in the table, the Franck–Condon factors calculated by using their potential function are very small and the ratios obtained do not reproduce the observed vibrational dependency of Γ. These discrepancies are due to that the D' potential curve reported by them crosses at the bond length much longer than the equilibrium position.

There may be two possibilities to explain the disagreement. First is that the D' potential curve reported by them is not accurate at high energy region. Second is that the potential curve obtained in the present work is not assigned to the

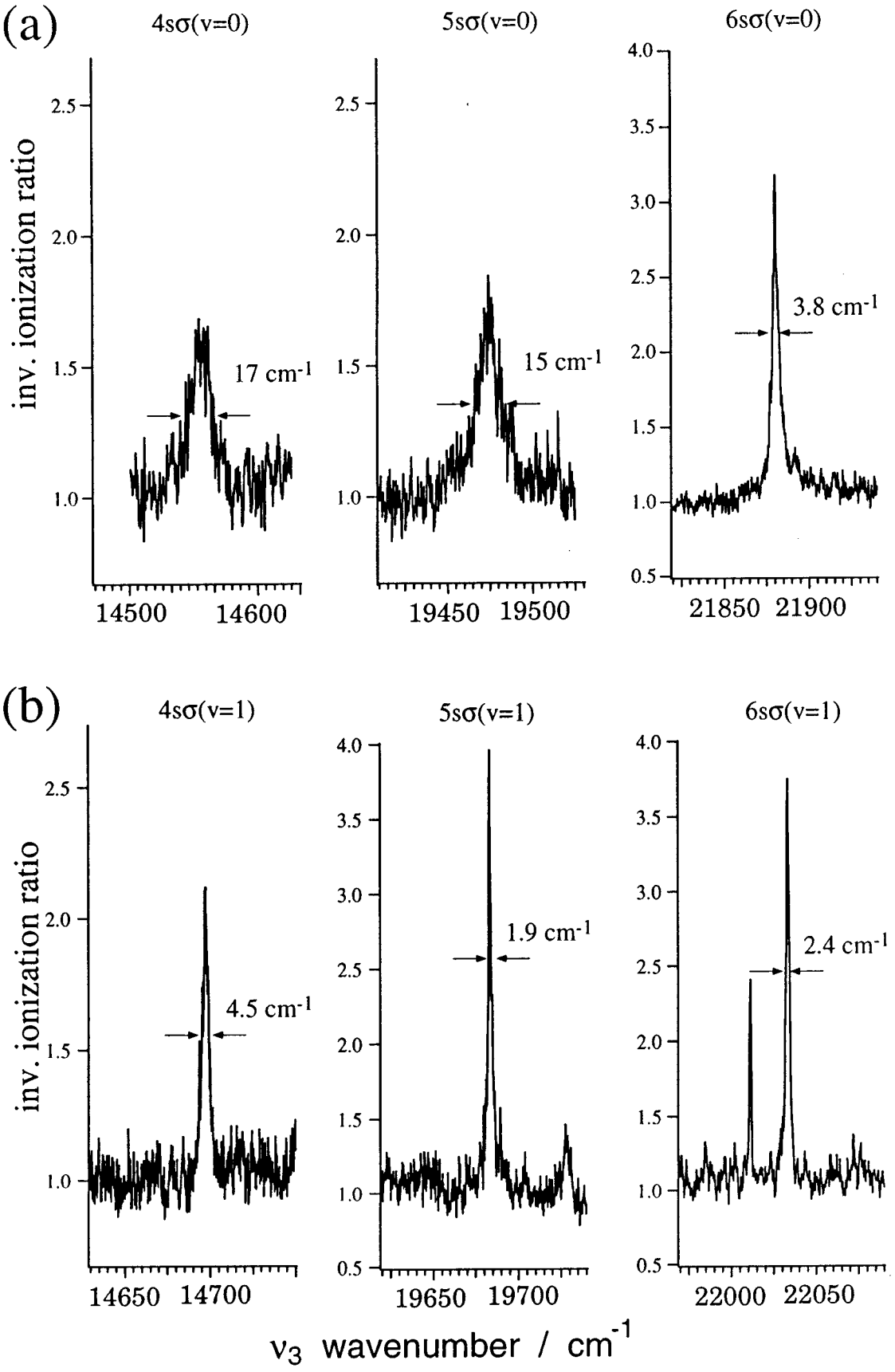

FIG. 10. Inverse ionization ratio spectra of (a) $ns\sigma(v=0)\leftarrow B(v=0)$ and (b) $ns\sigma(v=1)\leftarrow B(v=1)$ transitions.

TABLE II. Calculated $ns\sigma \leftrightarrow$repulsive state Franck–Condon factors, observed linewidths (Γ_{obs}), lifetimes (τ), and ratios of Γ_{obs} between $v=0$ and 1 levels.

	$4s\sigma$			$5s\sigma$			$6s\sigma$		
	FC factor (10^{-5} cm)	Γ_{obs} (cm^{-1})	τ (10^{-12} s)	FC factor (10^{-5} cm)	Γ_{obs} (cm^{-1})	τ (10^{-12} s)	FC factor (10^{-5} cm)	Γ_{obs} (cm^{-1})	τ (10^{-12} s)
$v=0$	5.8[a] 0.00[b]	17	0.31	6.3[a] 0.004[b]	15	0.35	5.1[a] 0.02[b]	3.8	1.4
$v=1$	1.5[a] 0.03[b]	4.5	1.2	0.85[a] 0.39[b]	1.9	2.7	2.4[a] 0.87[b]	2.4	2.2
$v=0/v=1$	3.8[a] 0.0[b]	3.8		7.5[a] 0.01[b]	7.9		2.1[a] 0.02[b]	1.6	

[a]For the repulsive potential curve, $V(R)=2.761\times10^{9}\exp(-10.8R)$ cm^{-1}.
[b]For the repulsive potential curve, $V(R)=1.3939\times10^{9}\exp(-9.1348R)$ cm^{-1} (Ref. 9) were used (see text).

D' state but to other repulsive state. According to the calculation by O'Neil *et al.*, the second excited $^1\Pi$ state is repulsive and crosses with the Rydberg states at shorter bond length than the D' state.[32] Very recently, Hiyama and Nakamura also obtained the second $^1\Pi$ potential curve by *ab initio* calculation and reported that the potential curve closely resembles with the potential curve obtained in the present work.[33] Therefore, it is possible that the repulsive curve observed in the present experiment is not the D' state but the second excited $^1\Pi$ state.

We also obtained the electronic matrix element H^e for each state, by substituting the observed Γ and the calculated $|\langle\chi_{v,J}(R)|\chi_{E,J}(R)\rangle|^2$ value into Eq. (13), which is listed in Table III. As can be seen in Table III, H^e is in the magnitude of a few hundreds wave number and decreases with the increase of n. Since H_n^e is thought to depend on $(n^*)^{-3/2}$, which is the scaling factor of the Rydberg orbital, the value $H_n^e\times(n^*)^{3/2}$ will be the same for the $4s\sigma-6s\sigma$ states, if a single repulsive state is involved for the predissociation. In Table III are also listed the values of $H_n^e\times(n^*)^{3/2}$, which are roughly the same. This result indicates that only a single repulsive state is responsible for the predissociation of the $ns\sigma$-Rydberg states. For the complete analysis of the Rydberg-valence interactions, the theoretical treatment with the close coupling method and MQDT method may be necessary.

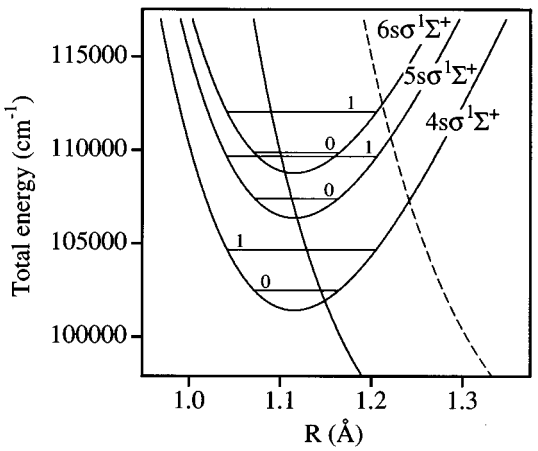

FIG. 11. Diabatic potential energy curves of the ns-Rydberg and the repulsive states. Solid curve, $V(R)=2.761\times10^{9}\exp(-10.8R)$ cm^{-1}, dashed curve, $V(R)=1.3939\times10^{9}\exp(-9.1348R)$ cm^{-1} (see Ref. 9). R is in units of angstrom. The origin of the energy is chosen to be the minimum of the ground state potential.

D. $5p$, $6p$, and $7p$ Rydberg states ($v=0$)

In the previous paper, we reported term values, rotational constants, and the energy differences between the σ and π components of the $v=1$ level of the $5-7p$ Rydberg states observed by the ion-dip spectroscopy. For the $v=0$ level, both the σ and π components were rotationally analyzed for the states up to $5p$ in the one-photon absorption spectrum.[4] However, only the σ component has been observed for $6p(v=0)$ and none of the analysis has been performed for $7p(v=0)$. Very recently, Ubachs and co-workers observed the resonance enhanced MPI spectra of the $v=0$ level of the $5p$ and $6p$ states.[20,21] However, only the σ-component was rotationally resolved and the rotational analysis of the π-component has not still been done. In the present work, we observed the $5p-7p(v=0)$ states by ion-dip spectroscopy and carried out their rotational analysis.

Figure 12 shows the ion-dip spectra of the $5p(v'=0,J')\leftarrow B\ ^1\Sigma^+(v''=0,J'')$ transition. The dips at $\nu_3\sim20\,260$ cm^{-1}, which are overlapped with a broad dip, are assigned to the P and R branches of the $5p\sigma\ ^1\Sigma^+(v'=0)\leftarrow B\ ^1\Sigma^+(v''=0)$ transition. The term value and the rotational constant was obtained by plotting total energy level vs $J(J+1)$ and $T_\Sigma=107\,175$ cm^{-1}, $\delta=0.669$, and $B=2.07$ cm^{-1} were obtained for $5p\sigma(v=0)$, which are listed in Table IV.

The assignment of the $5p\pi\ ^1\Pi(v=0)$ state is rather complicated. Two $^1\Pi\leftarrow X\ ^1\Sigma^+$ bands were observed in the one-photon absorption spectrum in the region of the $5p\pi(v=0)$ state and their rotational constants are anomalously small (1.517 and 1.650 cm^{-1}).[4] In the ion-dip spectrum, we also observed two groups of the P, Q, and R branches at $\nu_3\sim20\,410$ cm^{-1} and $\sim20\,490$ cm^{-1}, as shown in Fig. 12. They are assigned to the same $^1\Pi\leftarrow{}^1\Sigma^+$ transitions observed in the absorption spectra.[4] Both the two P, Q, and R

TABLE III. Electronic matrix element, H^e, and $(n^*)^{3/2}H^e$ for the $4-6s\sigma\leftrightarrow$repulsive state interaction. n^* is the effective principal quantum number.

	$4s\sigma$	$5s\sigma$	$6s\sigma$
H^e (cm^{-1})	220	180	110
$(n^*)^{3/2}H^e$ (cm^{-1})	1200	1490	1270

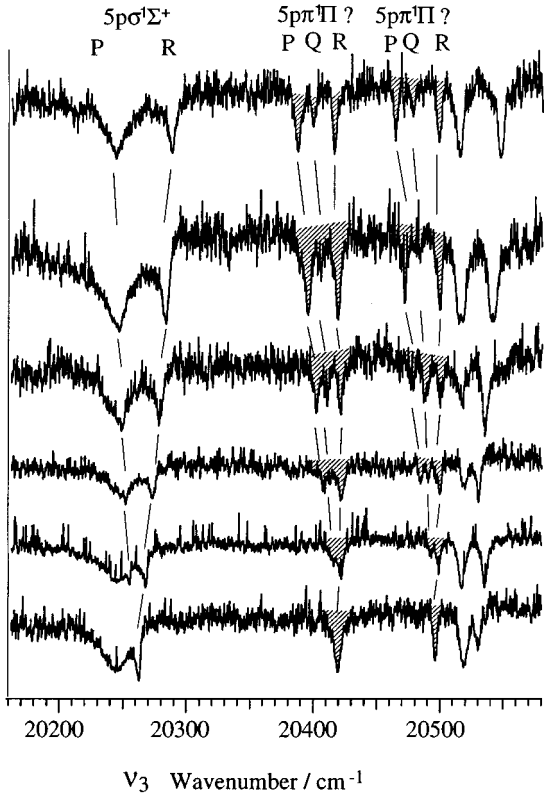

FIG. 12. Triple resonant ion-dip spectra of CO in the region of the $5p(v=0,J')\leftarrow B\ ^1\Sigma^+(v=0,J'')$ transition.

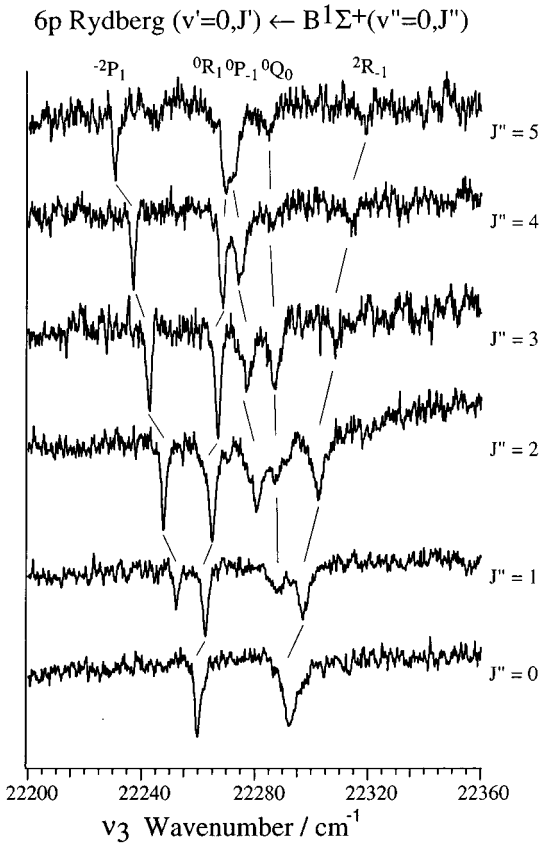

FIG. 13. Triple resonant ion-dip spectra of CO in the region of the $6p(v=0,J')\leftarrow B\ ^1\Sigma^+(v=0,J'')$ transition.

branches shade to red with the increase of J'' and $B=1.37$ for the lower electronic state and 1.54 cm^{-1} for the upper state, which are smaller than those reported. The best way to determine which state will be the $5p\pi\ ^1\Pi$ state is to examine Λ-type doubling. However, the observed Λ-type splitting were found to be smaller than the spectral linewidth of ν_3 laser (1 cm^{-1}). Therefore, the experiments with narrow band lasers are necessary for the assignment of the $5p\pi(v=0)$ state.

Figures 13 and 14 show the ion-dip spectra of the

$$6p(v'=0,J')\leftarrow B\ ^1\Sigma^+(v''=0,J'')$$

and

$$7p(v'=0,J')\leftarrow B\ ^1\Sigma^+(v''=0,J'')$$

transitions, respectively. As shown in the figures, the $6p$ and $7p$ states $(v=0)$ are rotationally well resolved and other states were not observed in these energy regions. Since the $6p$ and $7p$ states can be classified to the Hund's case (d), the

TABLE IV. Molecular constants of the observed $np\sigma\ ^1\Sigma^+(v=0)$ and $np\pi\ ^1\Pi(v=0)$ states. For comparison, term values reported by three groups are also given. All the values of the $4p\sigma$ and $p\pi$ states are adopted from Eidelsberg *et al.* (Ref. 4).

								Reported term value (cm^{-1})		
n		T_Λ (cm^{-1})	δ	B (cm^{-1})	C (cm^{-1})	ΔG (cm^{-1})	δG (cm^{-1})	Ogawa *et al.*[b]	Eidelsberg *et al.*[a]	Eikema *et al.*[c]
4[a]	$p\sigma$	103 054.07	0.683	1.92		2204	+20	103054	103054.07	103054.71
	$p\pi$	103 271.3	0.646	1.98	217.2	2134	−50	103272	103271.3	
5	$p\sigma$	107 175	0.669	2.07		2178	−6	107162	107174.1	107174.44
	$p\pi$	107 336	0.608	1.37	161.0	2152	−34	107215	107335.0	
	$p\pi$	107 413	0.582	1.54	238.5	2075	−109		107401.9	
6	$p\sigma$	109 173	0.663	1.70		2176	−8	109185	109172.79	109173.68
	$p\pi$	109 209	0.638	1.84 (2.14)[d]	35.8	2188	+4	109204	109202	
7	$p\sigma$	110 299	0.656	1.82		2177	−7	110310		
	$p\pi$	110 350	0.595	1.74 (1.92)[d]	52.0	2157	−27	110331		

[a]Reference 4.
[b]Reference 6.
[c]Reference 20.
[d]Rotational constants for both of the Π^+ and Π^- components are given.

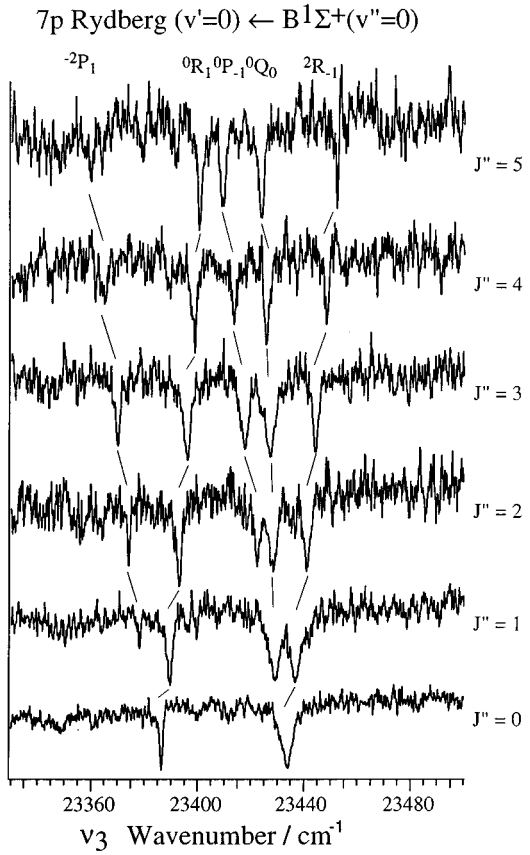

FIG. 14. Triple resonant ion-dip spectra of the $7p(v=0,J')$ $\leftarrow B\ ^1\Sigma^+(v=0,J'')$ transition of CO.

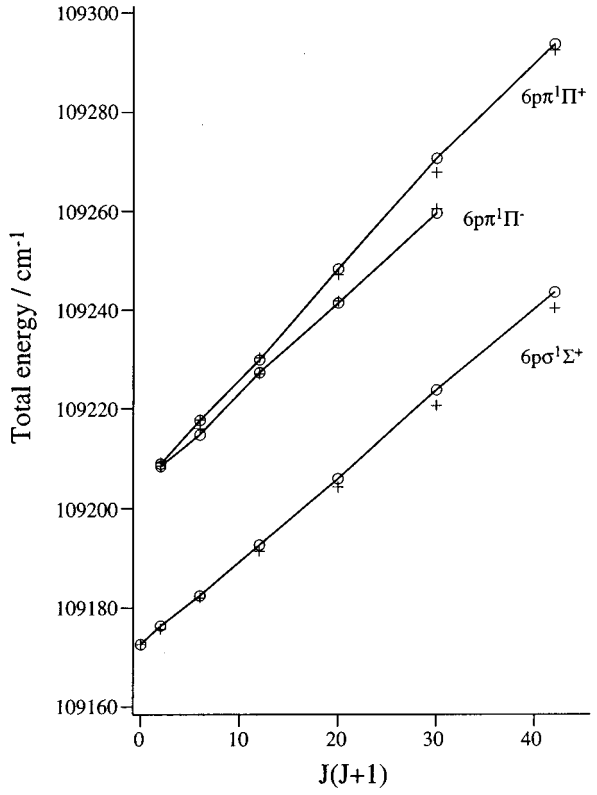

FIG. 15. Plot of the energy levels of the $6p(v=0)$ Rydberg state vs $J(J+1)$. ○, Observed levels; +, calculated energy levels by using the l-uncoupling model (see text).

rotational branches are labeled by the $^{N^{+\prime}-N''}\Delta J_{L'}$ expression. Here, N'' and $N^{+\prime}$ are the angular momenta of the B state and the ion core, respectively, and L' is the projection of the angular momentum of the Rydberg electron onto the rotational axis of the high Rydberg state. The rotational energy levels in the $6p$ and $7p$ states ($v=0$) are shown in Figs. 15 and 16, respectively. The rotational energy levels were analyzed by the l-uncoupling model as was described in previous papers.[25] T_Σ, δ, B, and $C(=T_\Lambda-T_\Sigma)$ for the $6p(v=0)$ and $7p(v=0)$ states are listed in Table IV. The calculated energy levels are also plotted in Figs. 15 and 16. The value of the effective angular momentum of the Rydberg electron, l, was obtained to be 0.8 from the analysis of the rotational structure of the np state. Ebata *et al.* also reported $l=0.8$ for both the $8p(v=1)$ and $9p(v=1)$ states[24] and the smaller value of l than unity for the $5-7p(v=1)$ was also reported.[25] Therefore, almost all the np-Rydberg states seems to be mixed with other electronic states having a low electronic angular momentum, such as ns-Rydberg states or valence states.

In the $v=1$ level of the np-Rydberg state which was reported in the previous paper,[25] it was found that the $\Sigma-\Pi$ energy separation ($=C$) decreases with n and a linear relationship was obtained between C and n^{-3}, as expected from the Rydberg formula. The C value decreases generally with the increase of n, which reflects the l-uncoupling, that is, a switching from Hund's case (b) to (d). In the $v=0$ level studied in the present work, however, a deviation from this relationship was found. The C value for the $6p(v=0)$ state obtained in the present experiment is 36 cm^{-1}. We also obtained $C=33$ cm^{-1} from the reported term values by Eidelsberg *et al.*,[4] which agrees well with the present results. By the same procedure, we obtained $C=51$ cm^{-1} for $7p(v=0)$ and it is larger than that of $6p(v=0)$. This means that the l-uncoupling is more extensive in $6p$ than in $7p$. The anomalous l-uncoupling is clearly seen in Figs. 13 and 14; the separation among the $^0R_1$, $^0P_{-1}$, and $^0Q_0$ branches of $6p(v=0)$ is much smaller than that of $7p(v=0)$. Therefore, the $C-n^{-3}$ relationship is not held in the $v=0$ level, which is different from the $v=1$ level.

The anomalous behavior of the $v=0$ level of the np-Rydberg states are also recognized when we plot the quantum defect vs $1/n^{*2}$, so-called Edlén plot. Here n^* $(=n-\delta)$ is the effective principal quantum number. In Fig. 17, (a) and (b) show the Edlén plots for the $np\sigma$ and $np\pi$ ($v=0,1$) states, respectively. As seen in the figure, while $\delta_{p\sigma}$ decreases smoothly with n^* in both $v=0$ and $v=1$ levels, a significant deviation is seen for $\delta_{p\pi}$ of the $v=0$ level of $7p\pi$ and $5p\pi$. The result indicates that the $np\pi$ states are perturbed at $5p-7p$ states. Since both e and f-symmetry components are perturbed, the perturbing state may have the same symmetry, that is $^1\Pi$. This state is either the second $^1\Pi$ state discussed in the previous section or the $W\ ^1\Pi$ state. For the $W\ ^1\Pi$ state, up to the $v=3$ level was observed by one-photon absorption.[4] The vibrational spacing is irregular and

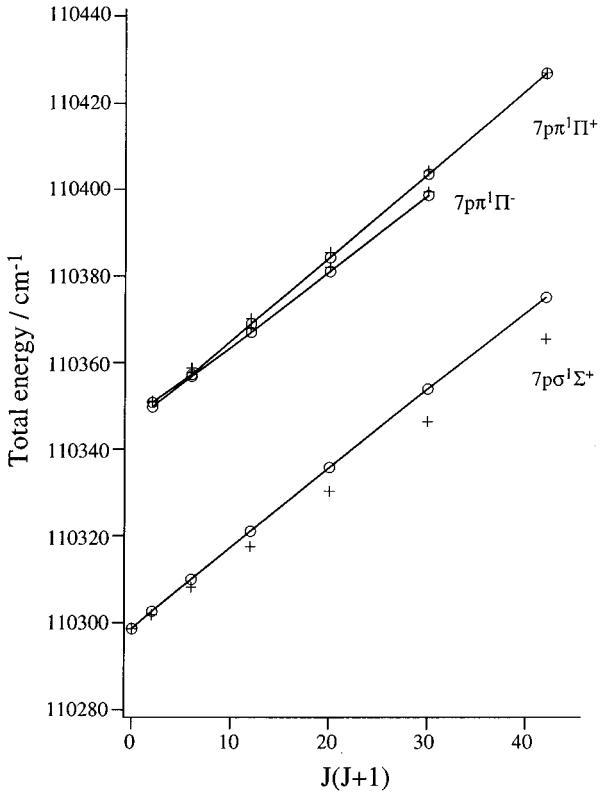

FIG. 16. Plot of the energy levels of the $7p(v=0)$ Rydberg state vs $J(J+1)$. ○, Observed levels; +, calculated energy levels by using the l-uncoupling model.

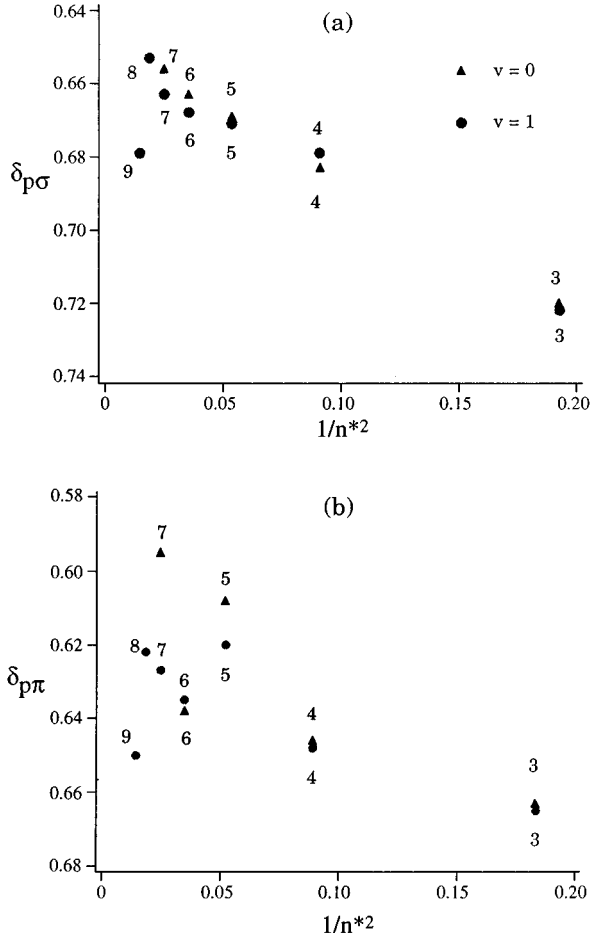

FIG. 17. Edlén plot for the np-Rydberg states ($v=0$ and 1). The quantum defects of $n=3$ and 4 were obtained by Eidelsberg *et al.* (Ref. 4) and $n=8$ and 9 by Ebata *et al.* (Ref. 24). Δ, $v=0$ and ○, $v=1$. (a) Edlén plot for the $np\Sigma^1$, $J=0$ level. Solid line was calculated by setting the slope to be -0.318 and the intersect to be 0.657. (b) Edlén plot for the $np\pi\ ^1\Pi^-$, $J=1$ level. Solid line was drawn by setting the slope -0.199 and the intersect to be 0.626.

the lifetime becomes short at $v \geqslant 1$. Cooper and Kirby reported *ab initio* calculation and suggested the strong interaction between the $W\ ^1\Pi$ state and the $3p\pi E\ ^1\Pi$ state.[34]

E. 4*f*, 5*f*, and 6*f*($v=0$) Rydberg states

1. Rotational structure, energy levels, and perturbations

The analysis of the $v=1$ levels of the $4f-9f$ Rydberg states were carried out in previous papers.[24,25] In those studies, it was found that the electronic energy of the f-Rydberg states is well reproduced by the long range force model and the ionization potential of the $v=1$ level, IP($v=1$), was determined. It was also found that below IP($v=0$) the predissociation rate of the e-symmetry levels is much larger than that of the f-symmetry levels. It was suggested that the predissociation of the f-Rydberg state occur by the interaction with the $D'\ ^1\Sigma^+$ state which perturbs only the e-symmetry level. For the $v=0$ levels of the nf-Rydberg states, none of the spectroscopic study has been reported yet and we extended the similar study to the $v=0$ levels of the $4f-6f$ Rydberg states.

The ion-dip spectra of the $4f(v'=0,J')\leftarrow B\ ^1\Sigma^+(v''=0,J'')$ transition are observed at $\nu_3=19\,200$–$19\,250$ cm^{-1}, which are shown in Fig. 3 and also in Fig. 18 in an expanded scale. Similar to the $np(v'=1,J')\leftarrow B\ ^1\Sigma^+(v''=1,J'')$ transition, the rotational branches are labeled by $^{N^+{}'-N''}\Delta J_{L'}$ and the assignment of the rotational lines is given in Fig. 18. As seen in the figure, the spectra at $\nu_3=19\,220$–$19\,250$ cm^{-1} are overlapped by other transitions which are marked by asterisks. These marked rotational lines could not be assigned to transitions to the upper state and was assigned to the P, Q, and R branches to the $A\ ^1\Pi(v=2,J')$ state induced by the stimulated emission from the B state.

The energy levels of the $4f(v=0)$ state are plotted in Fig. 4. The observed levels are classified into each L ($=0$, ±1, ±2, and ±3) components. By the same treatment as was done in previous papers,[25] the rotational levels were analyzed by comparing with the calculated levels which were obtained by using basis sets of Hund's case (b) (l-uncoupling model). The values of $T_\Sigma=106\,107$ cm^{-1} and $C=5.7$ cm^{-1} were obtained for $4f(v=0)$ by fitting with calculated energy levels. Here, C is the difference of the electronic energy expressed in terms of Hund's case (b) limit, that is $C=(T_\Lambda-T_\Sigma)/\Lambda^2$. From the term value and the ionization potential which will be discussed later, the quantum defect

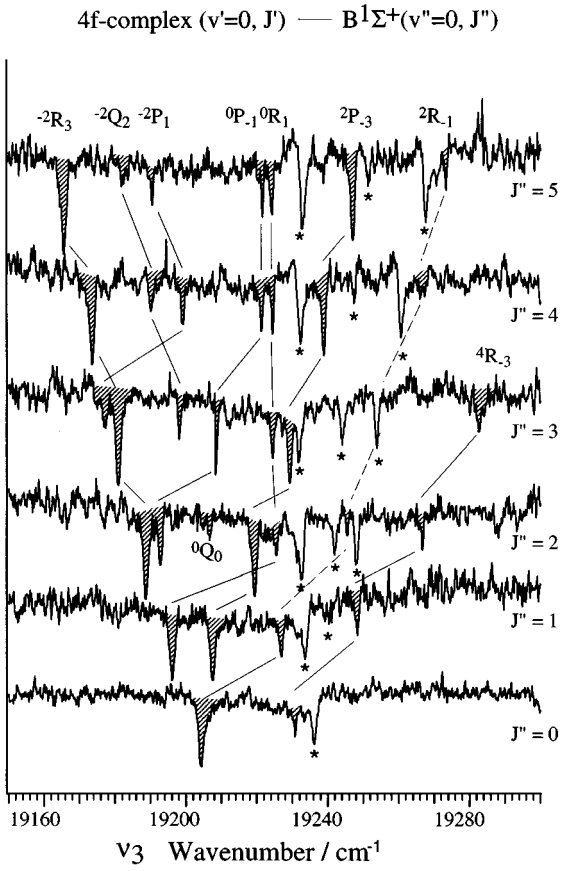

FIG. 18. Triple resonant ion-dip spectra of CO in the region of the $4f(v=0,J')\leftarrow B\ ^1\Sigma^+(v=0,J'')$ transition.

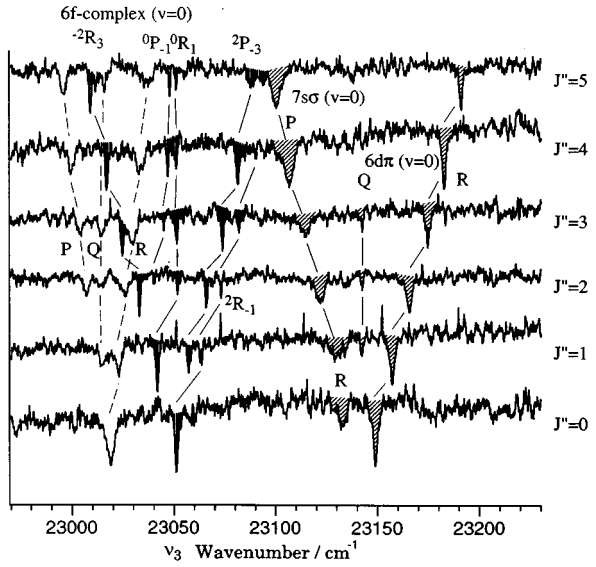

FIG. 19. Triple resonant ion-dip spectra of CO in the region of the $6f(v=0,J')$ and $7s-6d(v=0)\leftarrow B\ ^1\Sigma^+(v=0,J'')$ transitions.

was obtained to be $\delta=0.017$. These values are listed in Table V.

The ion-dip spectra of the $5f(v=0)\leftarrow B\ ^1\Sigma^+(v=0)$ transition are shown in Fig. 5 and that of the $6f(v=0)\leftarrow B\ ^1\Sigma^+(v=0)$ transitions is shown in Fig. 19. As shown in Fig. 6 and 21, both the transitions are rotationally well resolved and the assignments were performed by the same procedure done for the $4f(v=0)\leftarrow B\ ^1\Sigma^+(v=0)$ transition. The energy levels of the $5f(v=0)$ and $6f(v=0)$ states are shown in Figs. 7 and 22, respectively. From the analysis of rotational structure and by the comparison with the calculated energy levels, $T_\Sigma=108\,601\ \mathrm{cm}^{-1}$, $\delta=0.020$, and $C=3.7\ \mathrm{cm}^{-1}$ were obtained for the $5f(v=0)$ state and $T_\Sigma=109\,957\ \mathrm{cm}^{-1}$, $\delta=0.020$, and $C=1.6\ \mathrm{cm}^{-1}$ for the $6f(v=0)$ state.

TABLE V. Molecular constants of the observed $nf(v=0$ and 1) Rydberg states of CO.

nf	v	T_Σ (cm^{-1})	δ	C (cm^{-1})	ΔG (cm^{-1})	δG (cm^{-1})
$4f$	0	106 107	0.017	5.7		
	1	108 289	0.018	6.1	2182	−2
$5f$	0	108 601	0.020	3.2		
	1	110 783	0.021	3.7	2182	−2
$6f$	0	109 957	0.020	1.6		
	1	112 141	0.019	1.8	2184	0

As to the predissociation, we obtained the similar result for the $v=0$ level with that of the $v=1$ level reported previously.[25] As seen in Figs. 6, 20 and 21, almost all the intense dips appeared in the $4f$, $5f$, and $6f(v=0,J')\leftarrow B\ ^1\Sigma^+(v=0,J'')$ spectra were assigned to the transitions to the odd L components which belong to e-symmetry. Transitions to the even L components (f-symmetry) are observed very weakly. For example, In the $4f(v=0)\leftarrow B\ ^1\Sigma^+(v=0,J'')$ spectra, the $^0Q_0(2)$ line and the $^{-2}Q_2$ branch in the spectra of $J''=3$–5 is very weak. In the $5f(v=0)\leftarrow B\ ^1\Sigma^+(v=0,J'')$ spectra, the intensities of the $^{-2}Q_2$ and $^2Q_{-2}$ branches are also much weaker than that predicted. In the $6f(v=0)$ state, the f-symmetry components are completely missing. Therefore, the predissociation rate of the e-symmetry component is much larger than that of the f-symmetry component both in the $v=0$ and 1 levels and it may be concluded that the D' state is responsible for the predissociation.

In addition to the interaction with the D' valence state, we found several local perturbations for the nf-Rydberg states. For example, the intensity of the $^4R_{-3}$ branch of the $5f(v=0)-B(v=0)$ transition (Fig. 5) is anomalously strong at $J''=3$. As seen in Fig. 6, the intensity anomaly can be understood by the fact that the $J'=4$ level of the $L=-3$ component of $5f(v=0)$ is perturbed by the $5s\sigma\ ^1\Sigma^+(v=1)$ state. On the other hand, perturbation in the $5s\sigma\ ^1\Sigma^+(v=1)$ state was already reported in the previous paper though the perturbing state was not identified.[25] Both the $L=-3$ component of the $5f(v=0)$ state and the $5s\sigma\ ^1\Sigma^+(v=1)$ state belong to the e-symmetry and it is identified that both states are perturbing each other at $J\sim4$.

2. Ionization potential of $CO^+(v=0)$

Though the nf-Rydberg states are perturbed by the D' valence and other Rydberg states, the energy levels are essentially well described by the long range force model as was

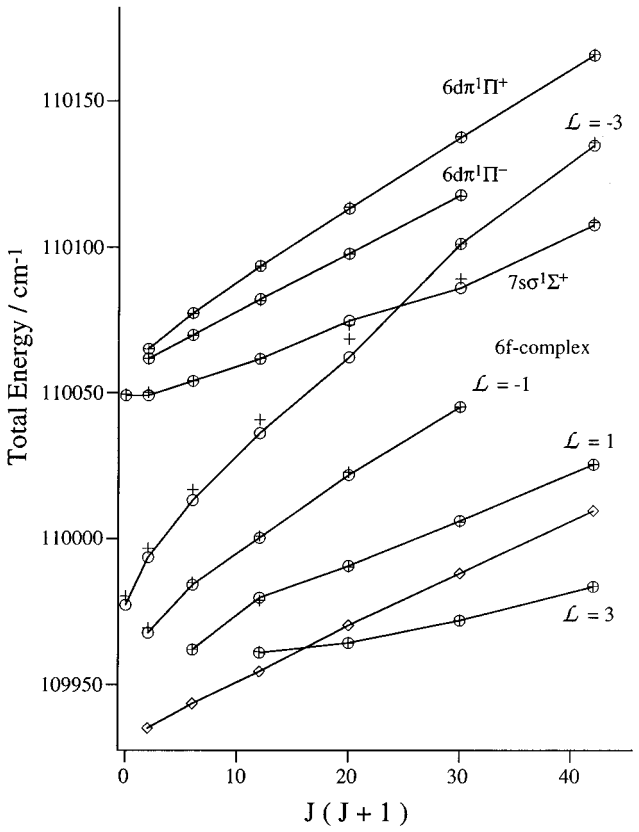

FIG. 20. Plot of the energy levels of $7s-6d(v=0)$ mixed state and the $6f(v=0)$ state vs $J(J+1)$. ○, observed; +, calculated energy levels by using the *l*-uncoupling model. In the calculation, the interaction between the $7s$ state with the $6f$ state is not included (see text).

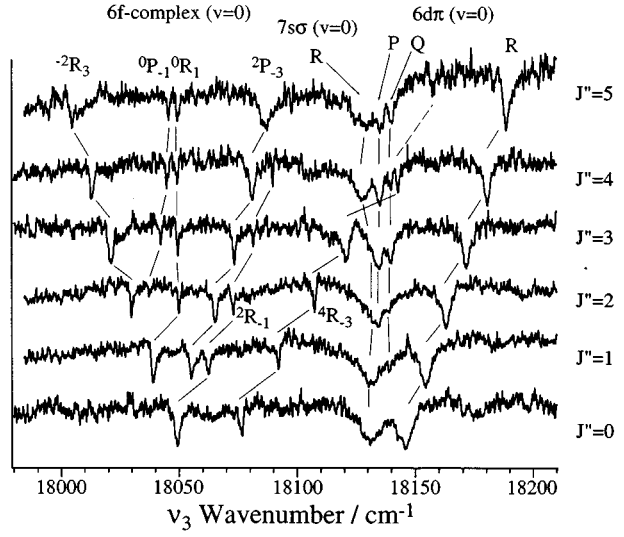

FIG. 21. Triple resonant ion-dip spectra of showing $6f(v=0,J')$ and $7s-6d(v=0)\leftarrow 3p\sigma C\ ^1\Sigma^+(v=0,J'')$ transitions.

reported for the $v=1$ level previously. In this model, the deviation from the hydrogenic Rydberg formula is calculated as the perturbation by the ion core having the quadrupole moment and the polarizability. This treatment was successfully applied to the $v=1$ level of the $8f$, $9f$-Rydberg state and the ionization potential, T_∞ $(v=1)$, the polarizability of the core, α, and the quadrupole moment of the core, Q_{zz}, were obtained.[24] The calculated energy levels well reproduced the observed ones of the lower Rydberg states ($4f$ and $5f$).[25]

For the $v=0$ level of the nf states, the same model was applied. In the present case, $T_\infty(v=0)=113\,025\pm2$ cm^{-1}, $\alpha=9\pm2$ a.u., and $Q_{zz}=0.96\pm0.08$ a.u. were obtained by using the observed values of T_Σ and C of the $5f(v=0)$ and $6f(v=0)$ states. Here, α and Q_{zz} are the polarizability and the quadrupole moment of the core, respectively. The calculated values for $4f(v=0)$ by using these value are $T_\Sigma=106\,106$ cm^{-1} and $C=5.9$ cm^{-1}, which agree very well with the observed ones. Very recently, Kong *et al.*[35] obtained the rotationally resolved PFI-ZEKE spectrum of the $v=0$ level of $CO^+(X\ ^2\Sigma^+)$ and obtained $T_\infty=113\,025.6\pm1.5$ cm^{-1} and the present value shows excellent agreement with their result. In one-photon absorption spectrum, the convergence limit of the $v=0$ series, $T_\infty=113\,029\pm2$ cm^{-1}, was obtained by Ogawa and Ogawa. The values of α and Q_{zz} are almost the same with those obtained for the $nf(v=1)$ states.[24]

F. Interaction among the $7s'\sigma(v=0)$, $6d\pi(v=0)$, and $6f(v=0)$ states

Since the quantum defect of $ns\sigma$ states is $\delta=\sim0.9$, the $7s\sigma\ ^1\Sigma^+(v'=0,J')\leftarrow B\ ^1\Sigma^+(v''=0,J'')$ transition is expected to occur at 100 cm^{-1} higher energy side of the $6f(v=0)\leftarrow B\ ^1\Sigma^+(v''=0,J'')$ transition. In Fig. 19, the $7s\sigma\ ^1\Sigma^+(v'=0,J')\leftarrow B\ ^1\Sigma^+(v''=0,J'')$ transition is observed at $\nu_3=23\,100$–$23\,150$ cm^{-1}. As can be seen in the figure, however, three rotational dips are observed in the spectra of $J''\geqslant1$ and they spread widely with J''. Therefore, the structure cannot be assigned to the simple $7s\sigma\ ^1\Sigma^+(v'=0,J')\leftarrow B\ ^1\Sigma^+(v''=0,J'')$ electronic transition. From the rotational analysis described below, it was found that this anomalous rotational structure is due to a strong mixing among $7s\sigma(v'=0)$, $6d\sigma(v'=0)$ and $6d\pi(v'=0)$ states. In Fig. 19, three dips are observed at $\nu_3=23\,100$–$23\,150$ cm^{-1} and they spread widely with the increase of J''. As was described in the previous paper, the $ns\sigma$ state strongly mixes with the $(n-1)d\sigma$ state and the mixed state interacts with the $(n-1)d\pi$ state by Λ-type doubling. The interaction changes not only the energy levels but also the transition intensity. In the present case, the $7s\sigma(v=0)$ state mixes with the $6d\sigma(v=0)$ state to form the mixed $7s'\sigma\ ^1\Sigma^+$ state. This state interacts only with the Π^+ component of the $6d\pi\ ^1\Pi$ state. Therefore, the rotational constant of the Π^- component is almost equal to that of the ion core, while the rotational constant of either the $^1\Sigma^+$ or the Π^+ state becomes larger and the other becomes smaller than that of the ion core depending on which state is higher in energy. Among the three dips observed at $\nu_3=21\,300$–$23\,200$ cm^{-1}, the dip shifting to red with J'' is broader than other two dips. We assigned this dip to the P branch of the $7s'\sigma\ ^1\Sigma^+(v'=0,J')\leftarrow B\ ^1\Sigma^+(v''=0,J'')$ transition because the ion-dip spectra of the other $ns\sigma$ states were broad. On the other hand, the R branch corresponding to the $7s'\sigma\leftarrow B$ transition is missing. The dip observed at $\nu_3=23\,140$ cm^{-1} is assigned to the Q branch to the Π^- com-

ponent of the $6d\pi\ ^1\Pi$ state. The third dip at ν_3=23 150–23 180 cm^{-1} which shifts to blue with J'' is assigned to the R branch to the Π^+ component of the $6d\pi\ ^1\Pi$ state.

To investigate further the rotational structure of this mixed states we observed the similar ion-dip spectra by changing the intermediate state from $3s\sigma B\ ^1\Sigma^+(v=0)$ to $3p\sigma C\ ^1\Sigma^+(v=0)$ which is shown in Fig. 21. As was expected from the selection rule of $\Delta l=\pm 1$, intense dips are observed for the ns, $nd(v'=0)\leftarrow 3p\sigma C\ ^1\Sigma^+(v''=0)$ transitions. However, the relative intensity is quite different from the spectrum of Fig. 19. The broad R branch of the $7s'\sigma(v=0)\leftarrow 3p\sigma C\ ^1\Sigma^+(v''=0)$ transition is observed at $\nu_3\sim$18 130 cm^{-1}. On the other hand, corresponding P branch is missing in Fig. 21. For the $6d\pi(v=0)$ state, the P and Q branches are seen at $\nu_3\sim$181 30 cm^{-1}, while the R branch shifts to blue with J''. The energy levels obtained from Figs. 21 and 23 agree well and they are shown in Fig. 20. By the strong l-uncoupling, both the $6d\pi\ ^1\Pi^+$ and $^1\Pi^-$ components are widely separated. The obtained values are B=2.49 cm^{-1} and B=1.99 cm^{-1} for $6d\pi\ ^1\Pi^+$ and $^1\Pi^-$, respectively, and B=1.3 cm^{-1} for $7s'\sigma$. The rotational constant for $^1\Pi^-$ component is almost the same as that of the ion core. T_Π=110 062 cm^{-1} and $\delta_{6d\pi}=-0.083$ for the $6d\pi(v=0)$ state and T_Σ=110 049 cm^{-1} and $\delta_{7s'\sigma}$=0.928 for $7s'\sigma(v=0)$. The value of $\delta_{6d\pi}$ for $6d\pi(v=0)$ is smaller than that for $3d\pi(v=0)(\delta_{3d\pi}=-0.0244)$.[4]

It is expected that the angular momentum l of the $6d$-Rydberg electron is much smaller than 2 because of the $7s-6d$ mixing. To investigate the $7s'\sigma\ ^1\Sigma^+-6d\pi\ ^1\Pi$ interaction, we applied the analysis similar to that used for the $3d\sigma-3d\pi$ perturbation of NO done by Huber and Miescher.[36] The difference of the energy between $6d\pi\ ^1\Pi^+(E'_\pi)$ and $7s'\sigma\ ^1\Sigma^+(E'_\Sigma)$ states is expressed by following equation:

$$(E'_\pi-E'_\Sigma)^2=4\alpha^2J(J+1)+C^2, \tag{15}$$

where the parameter α is given by

$$\alpha^2=2B^2l(l+1). \tag{16}$$

So, by plotting $(E'_\pi-E'_\Sigma)^2$ against $J(J+1)$, α can be obtained from the slope. Figure 22 shows the plot of $(E'_\pi-E'_\Sigma)^2$ vs $J(J+1)$ for the $7s'\sigma(v=0)-6d\pi(v=0)$ interaction. From the value of the slope (77 cm^{-2}), α is obtained to be 4.4 cm^{-1}, which is much smaller than α=6.86 cm^{-1} of the pure d-Rydberg state. Calculated energy levels by using the obtained value of α are also plotted in Fig. 20, which agree well with the observed energy levels.

It was also found that the mixed $7s'\sigma\ ^1\Sigma^+(v=0)$ state is further perturbed locally by the $6f(v=0)$ Rydberg state. As shown in Fig. 20, the J=4 and 5 levels of the $7s\sigma(v=0)$ state deviate from the energy levels calculated by considering the $7s-6d$ mixing described above. On the other hand, the $L=-3$ component of the $6f(v=0)$ state significantly shifts to red at J'=4 from the levels calculated without including the perturbation. As was described in previous papers, similar local perturbation between nf and $(n+1)s$ was also reported for the v=1 level by Ebata *et al.*[24]

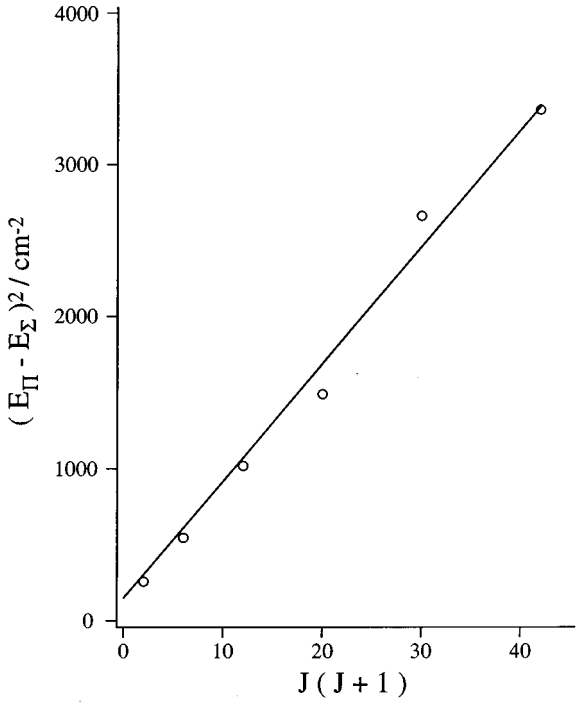

FIG. 22. Plot of $(E_{\Pi'}-E_{\Sigma'})^2$ vs $J(J+1)$ for the $7s'\sigma\ ^1\Sigma^+(v=0)-6d\pi\ ^1\Pi^+(v=0)$ mixed states.

G. $W\ ^1\Pi(v=2)$ state

Besides the Rydberg states converging to the ground state of CO ion, we observed another transitions in the ion-dip spectrum. In Fig. 3, the intense dips are observed between the $4f(v=0)$ and $5s\sigma(v=0)$ states. They are assigned to the P, Q, and R branches of the $W\ ^1\Pi(v'=2,J')\leftarrow 3s\sigma B\ ^1\Sigma^+(v''=0,J'')$ transition. The $W\ ^1\Pi$ state was observed in the one-photon absorption spectrum[4] and by REMPI with an extreme-ultraviolet laser source.[21] Also, the same transition was observed by fluorescence depletion spectroscopy.[22] The $W\ ^1\Pi$ state is the first member of the $ns\sigma$ Rydberg series converging to the $A\ ^2\Pi$ excited state of the CO^+, and $W\ ^1\Pi\leftarrow B\ ^1\Sigma^+$ is the allowed transition corresponding to $1\pi\rightarrow 5\sigma$ with fixed $3s\sigma$. By the measurement of the linewidth, J dependent predissociation is reported.[21,22]

IV. CONCLUSION

By using ion-dip spectroscopy with triple-resonant excitation, four Rydberg states (ns, np, nd, and nf) with v=0 and 1 were observed and their rotational structures were analyzed. It was found that the energy levels of the nf-Rydberg states are well explained by the long range force model and that the e-symmetry components selectively predissociates through the interaction with the D' valence state. The interaction between the ns-Rydberg and a repulsive state were also analyzed, and the interaction matrix element and the potential curve of the repulsive state was obtained in the energy region of 98 000–112 000 cm^{-1}. We cannot conclude, however, that whether the obtained repulsive potential curve is due to the D' state at this moment. In addition to the

Rydberg-valence interaction, the Rydberg–Rydberg interaction was found. The $nd\sigma$ state mixes with the $(n+1)s\sigma$ state to form the admixture state which interacts with the $nd\pi$ state by Λ-type doubling. The local interaction between the $(n+1)s\sigma$ state and the nf-state were also observed. For the future work, the detection of the photofragment, that is C and/or O atom, would be an important investigation to reveal the mechanism and the dynamics of the predissociating Rydberg states.

[1] C. Letzelter, M. Eidelsberg, F. Rostas, J. Breton, and B. Thieblemont, Chem. Phys. **114**, 273 (1987).
[2] G. Stark, K. Yoshino, P. L. Smith, K. Ito, and W. H. Parkinson, Astrophys. J. **369**, 574 (1991); **395**, 705 (1992).
[3] M. Eidelsberg, J. Y. Roncin, A. Le Floch, F. Launay, C. Letzelter, and J. Rostas, J. Mol. Spectrosc. **121**, 309 (1987).
[4] M. Eidelsberg and F. Rostas, Astron. Astrophys. **235**, 472 (1990).
[5] M. Eidelsberg, J. J. Banayoun, Y. Viala, and F. Rostas, Astron. Astrophys. Suppl. Ser. **90**, 231 (1990).
[6] M. Ogawa and S. Ogawa, J. Mol. Spectrosc. **41**, 393 (1972).
[7] S. Ogawa and M. Ogawa, J. Mol. Spectrosc. **49**, 454 (1974).
[8] D. M. Cooper and S. R. Langhoff, J. Chem. Phys. **74**, 1200 (1981).
[9] W. ÜL. Tchang-Brillet, P. S. Julienne, J.-M. Robbe, C. Letzelter, and F. Rostas, J. Chem. Phys. **96**, 6735 (1992).
[10] T. Masaki, Y. Adachi, and C. Hirose, Chem. Phys. Lett. **139**, 62 (1987).
[11] S. Sekine, T. Masaki, Y. Adachi, and C. Hirose, J. Chem. Phys. **89**, 3951 (1988).
[12] S. Sekine, Y. Adachi, and C. Hirose, J. Chem. Phys. **90**, 5346 (1989).
[13] S. Sekine, S. Iwata, and C. Hirose, Chem. Phys. Lett. **180**, 173 (1991).
[14] F. Merkt and T. P. Softley, Chem. Phys. Lett. **165**, 477 (1990); Mol. Phys. **72**, 787 (1991).
[15] K. Tsukiyama, M. Momose, M. Tsukakoshi, and T. Kasuya, Opt. Commun. **79**, 88 (1990).
[16] P. Klopotek and C. R. Vidal, Opt. Soc. Am. B **2**, 869 (1985).
[17] A. Fujii, T. Ebata, and M. Ito, Chem. Phys. Lett. **161**, 93 (1989).
[18] M. A. Hines, H. A. Michelsen, and R. N. Zare, J. Chem. Phys. **93**, 8557 (1990).
[19] P. F. Levelt, W. Ubachs, and W. Hogervorst, J. Chem. Phys. **97**, 7160 (1992); J. Phys. II France **2**, 801 (1992).
[20] K. S. E. Eikema, W. Hogervorst, and W. Ubachs, Chem. Phys. **181**, 217 (1994).
[21] W. Ubachs, K. S. E. Eikema, P. F. Levelt, W. Hogervorst, M. Drabbels, W. L. Meerts, and J. J. ter Meulen, Astrophys. J. **427**, 55 (1994).
[22] M. Drabbels, J. Heinze, J. J. ter Meulen, and W. L. Meerts, J. Chem. Phys. **99**, 5701 (1993).
[23] N. Hosoi, T. Ebata, and M. Ito, J. Phys. Chem. **95**, 4182 (1991).
[24] T. Ebata, N. Hosoi, and M. Ito, J. Chem. Phys. **97**, 3920 (1992).
[25] M. Komatsu, T. Ebata, and N. Mikami, J. Chem. Phys. **99**, 9350 (1993).
[26] S. G. Tilford and J. T. Vnderslice, J. Mol. Spectrosc. **26**, 419 (1968).
[27] K. P. Huber and G. Herzberg, *Molecular Spectra and Molecular Structure IV, Constants of Diatomic Molecules* (Van Nostrand, Reinhold, 1979).
[28] See Ref. 27, Fig. 17.
[29] H. Zacharias, R. Schmeidl, and K. H. Welge, Appl. Phys. **21**, 127 (1980).
[30] H. Lefebre-Brion and R. W. Field, *Perturbations in the Spectra of Diatomic Molecules* (Academic, New York, 1986).
[31] J. Tellinghuisen, Adv. Chem. Phys. **60**, 299 (1985).
[32] S. T. O'Neil and H. F. Sahafer III, J. Chem. Phys. **53**, 3994 (1970).
[33] M. Hiyama and H. Nakamura (private communication).
[34] D. L. Cooper and K. Kirby, Chem. Phys. Lett. **152**, 393 (1988).
[35] W. Kong, D. Rodgers, J. W. Hepburn, K. Wang, and V. McKoy, J. Chem. Phys. **99**, 3159 (1993).
[36] K. P. Huber and E. Miescher, Helv. Phys. Acta **36**, 257 (1963).
[37] E. Lindholm, Ark. Fys. **40**, 103 (1969).